# Fast and Fully Automatic Left Ventricular Segmentation and Tracking in Echocardiography Using Shape-Based B-Spline Explicit Active Surfaces

João Pedrosa*, Sandro Queirós*†, Olivier Bernard‡, Jan Engvall§, Thor Edvardsen¶, Eike Nagel||, Jan D'hooge*
*Laboratory on Cardiovascular Imaging and Dynamics, KU Leuven, Belgium; †ICVS/3Bs PT Government Associate Laboratory and the Algoritmi Center, University of Minho, Portugal; ‡CREATIS, Centre national de la recherche scientifique, Inserm, INSA-Lyon, University of Lyon, University of Lyon 1, Villeurbanne, France; §Department of Clinical Physiology and Department of Medical and Health Sciences, Linköping University, Linköping, Sweden; ¶Center for Heart Failure Research, University of Oslo, Norway. Department of Cardiology, Oslo University Hospital, Rikshospitalet, Norway; ||Institute for Experimental and Translational Cardiovascular Imaging, University Hospital Frankfurt/Main, DZHK Centre for Cardiovascular Imaging, Frankfurt, Germany.

***Abstract*—Cardiac volume/function assessment remains a critical step in daily cardiology and 3D ultrasound plays an increasingly important role. Fully automatic left ventricular segmentation is, however, a challenging task due to the artifacts and low contrast-to-noise ratio of ultrasound imaging. In the present work, a fast and fully automatic framework for full cycle endocardial left ventricle segmentation is proposed. This approach couples the advantages of the B-spline explicit active surfaces framework, a purely image information approach, to those of statistical shape models to give prior information about the expected shape for an accurate segmentation. The segmentation is propagated throughout the heart cycle using a localized anatomical affine optical flow. It is shown that this approach not only outperforms other state-of-the-art methods in terms of distance metrics with mean average distances of $1.81 \pm 0.59$ mm and $1.98 \pm 0.66$ mm at end-diastole and end-systole respectively but is computationally efficient (in average 11 seconds per 4D image) and fully automatic.**

***Index Terms*—3D echocardiography, left ventricle segmentation, B-spline explicit active surfaces, statistical shape model, localized anatomical affine optical flow.**

## I. Introduction

ANALYSIS of cardiac function, and specifically of left ventricular (LV) function, is an important part of clinical cardiology for patient management, disease diagnosis, risk stratification or therapy selection [1], [2], [3]. Among the different cardiac imaging modalities, 3D ultrasonic imaging stands out as a low-cost, portable, risk-free and non-invasive technique with good space and time resolution. However, 3D ultrasound poses several challenges due to its low contrast-to-noise ratio, the presence of artifacts and the dependence on the acquisition conditions [4].

In spite of the challenges presented, numerous approaches have been proposed for automatic or semi-automatic chamber assessment, both in the research community and in the form of commercial solutions as can be appreciated in the review of Pedrosa et al. [5]. LV endocardial segmentation has been particularly well studied and a number of approaches have been proposed as can be appreciated in the review of Leung and Bosch [4]. This is especially true when compared to other chambers such as the right ventricle and left atrium which have received significantly less attention though some methods have been proposed [6], [7]. Given the different frameworks proposed for the same problem of LV segmentation, initiatives such as the CETUS challenge [8] play an extremely important role in allowing the benchmarking of different frameworks [9], [10], [11], [12], [13] on the same datasets using the same evaluation tools. Though the highest ranked solution of the challenge was a purely image information approach by Barbosa et al. [9] using the B-spline explicit active surfaces (BEAS) framework, later approaches using shape and/or appearance clues proved to be more successful. Such approaches by Oktay et al. [14] and van Stralen et al. [15] came to prove the pre-existing idea that 3D ultrasound imaging is inherently challenging to segment due to its many artifacts and that prior information is key to an accurate segmentation. Nevertheless, the gap between state-of-the-art technologies and interobserver variability is still present and, as such, new approaches joining the advantages of successful basic segmentation frameworks such as BEAS with tools that provide prior information about the LV are of much interest.

In the present work, a framework for fast and fully automatic segmentation and tracking of the LV in 3D echocardiographic images is proposed. A shape-based deformable model based on the BEAS framework [16] using a statistical shape model (SSM) as in Queirós et al. [17] is used for segmentation at end-diastole (ED). This assures that both image information and shape-based clues are used, thus increasing the robustness of this approach when compared to BEAS or other methods based solely on image information. This segmentation is then propagated to the rest of the cardiac cycle using localized anatomical affine optical flow (lAAOF) [18]. To further refine the results from the lAAOF, the shape-based BEAS framework is applied at end-systole (ES), again allowing for the combination of both image information and shape-based clues for the final segmentation result.

The main novelty of the presented study lies on the algorithmic design and validation of the proposed method. Joining different and independent algorithmic tools, the authors were able to build a single efficient framework capable of performing fast, fully automatic and robust full-cycle segmentation and validate it in a very reliable dataset that allows direct comparison to other state-of-the-art methods. Furthermore, the shape-based regularization introduced in [18] was extended in this study, from the original formulation based on a 1D SSM of Queirós et al. which would not be applicable to the LV to a full 2D oriented SSM.

## II. Methodology

### A. B-spline Explicit Active Surfaces

The key concept of the BEAS framework [16] is to regard the boundary of an object as an explicit function, where one of the coordinates of the points on the surface, $\mathbf{x} = \{x_1, ..., x_n\}$, is given explicitly as a function of the remaining coordinates, i.e. $x_1 = \psi(x_2, ..., x_n)$. In this framework, $\psi$ is defined as a linear combination of B-spline basis functions:

$$x_1 = \psi(x_2, ..., x_n) = \psi(\mathbf{x}^*) = \sum_{\mathbf{k} \in \mathbb{Z}^{n-1}} c[\mathbf{k}] \beta^d \left( \frac{\mathbf{x}^*}{h} - \mathbf{k} \right), \quad (1)$$

where $\mathbf{x}^*$ is the point of coordinates $\{x_2, ..., x_n\}$ and $\beta^d(\cdot)$ the uniform $(n\text{–}1)$-dimensional B-spline of degree $d$. The knots of the B-splines are located on a rectangular grid defined on the chosen coordinate system, with a regular spacing given by $h$. The coefficients of the B-spline representation are gathered in $c[\mathbf{k}]$.

Given the volumetric nature of the object of interest, the B-spline representation was created on a spherical coordinate system thus defining the active geometric functions as $r = \psi(\phi, \theta)$. As in previous implementations of BEAS for LV segmentation [19], the angular discretization of the boundary representation was set empirically at $24 \times 16$ (elevation$\times$azimuth) and the B-spline scale to $2^1$ for both angular coordinates.

The evolution of the model is defined by the minimization of an energy criterion $E$. This energy is expressed by the sum of the data attachment term $E_d$ and a regularization term $E_r$:

$$E = E_d + E_r. \quad (2)$$

The data attachment energy function $E_d$ follows a variation of the localized Yezzi energy adapted for endocardial segmentation [19], thus taking into account the expected intensities of the blood pool and the endocardium:

$$E_d = \int_\Omega \delta_\phi(\mathbf{x}) \int_\Omega B(\mathbf{x}, \mathbf{y}) \cdot (u_{in} - u_{out}) \, d\mathbf{y} d\mathbf{x}, \quad (3)$$

where $\delta_\phi(\mathbf{x})$ is the Dirac operator applied to the level set function $\phi(\mathbf{x}) = \Gamma(\mathbf{x}^*) - x_1$, which is defined over the image domain $\Omega$ and where $\Gamma(\mathbf{x}^*)$ represents the surface being segmented. $u_{in}$ and $u_{out}$ are the local intensity means around $x$, respectively inside and outside the surface. $B(\mathbf{x}, \mathbf{y})$ is the mask function in which these local parameters are estimated, restricted to the points along $\mathbf{N}(\mathbf{x})$, the normal direction of the surface, at a distance smaller than $\rho$:

$$B(\mathbf{x}, \mathbf{y}) = \begin{cases} 1, & if \quad \mathbf{y} = \mathbf{x} + k\mathbf{N}(\mathbf{x}), k \in [-\rho, \rho] \\ 0, & otherwise \end{cases} \quad (4)$$

The neighborhood region limit $\rho$ was set at 16 mm as in Barbosa et al. [9].

The minimization of the data attachment energy term in (3) can then be performed through optimization of the B-spline coefficient $c[\mathbf{k}_i]$, thus:

$$\frac{\partial E_d}{\partial c[\mathbf{k}_i]} = \int_\Gamma \left( \frac{\bar{I}(\mathbf{x}^*) - u_{in}}{A_{in}} + \frac{\bar{I}(\mathbf{x}^*) - u_{out}}{A_{out}} \right) \beta^d \left( \frac{\mathbf{x}^*}{h} - \mathbf{k}_i \right) d\mathbf{x}^*, \quad (5)$$

where $A_j$ is the area of region $j$ used to estimate the local mean $u_j$ and $\bar{I}(\mathbf{x}^*)$ corresponds to the image value at the position $\mathbf{x} = \{\Gamma(\mathbf{x}^*), x_2, ..., x_n\}$.

### B. Statistical Shape Model (SSM)

In order to provide accurate shape information to the proposed shape-based approach, a sufficiently broad and numerous dataset of 3D LV shapes is needed. For that purpose, 289 cardiac magnetic resonance (cMR) datasets from a large multi-center clinical study, DOPPLER-CIP [20], were used. This study was aimed at patients whose profile corresponds to suspected chronic ischemic disease and thus encompasses patients of a broad clinical spectrum. The cMR datasets were contoured by experts at ED and ES and the 2D slices were aligned using an iterative closest point (ICP) algorithm [21] to correct for breath-hold slice misalignment. A 3D mesh was then interpolated from the aligned 2D contours at ED and ES for each patient. A more detailed description of the strategy used to create the 3D LV meshes is provided in the supplementary files.

Similar to Queirós et al. [17], the SSM was built in the BEAS coordinate system; in this case in spherical coordinates. The SSM shapes will then be represented by their B-spline representation coefficients $c[\mathbf{k}]$. Because such a representation assumes that the position and orientation of the coordinate system is identical for every shape, the position and orientation of the training shapes have to be aligned, which can be done according to the centroid and direction of largest variance of each shape.

Starting from the aligned 3D LV shapes in BEAS space, the first step to build the SSM is to scale all shapes so that equivalent points from different shapes can be compared without the influence of the LV size. Considering $c_s[\mathbf{k}]$ the $s^{\text{th}}$ shape of all $N$ shapes, this is done by: calculating the mean of all shapes $\bar{c}[\mathbf{k}] = \frac{1}{N} \sum_{s=1}^{N} c_s[\mathbf{k}]$, scaling each shape to the current mean $\bar{c}[\mathbf{k}]$ and then repeating these steps until the process converges [22]. The scaling step is done according to:

$$c_{scaled}[\mathbf{k}] = c[\mathbf{k}] \frac{\sum_i w[\mathbf{k}_i] \bar{c}[\mathbf{k}_i] c[\mathbf{k}_i]}{\sum_i w[\mathbf{k}_i] c[\mathbf{k}_i] c[\mathbf{k}_i]}, \quad (6)$$

where $w[\mathbf{k}]$ is a set of weights chosen to give more significance to the points that tend to be most stable:

$$w[\mathbf{k}_i] = \left( \sum_{s=1}^{N} Variance(c_s[\mathbf{k}_i]) \right)^{-1}. \quad (7)$$

Principal Component Analysis (PCA) can then be applied to extract the shape variability of the LV B-spline coefficients

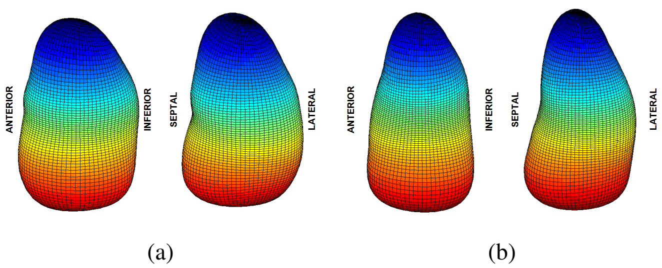


Fig. 1: SSM mean models at ED (a) and ES (b).

[22]. Through singular value decomposition [23], it is then possible to obtain the eigenvectors $\mathbf{p}_i$ and the corresponding eigenvalues $\lambda_i$ of the covariance matrix:

$$\mathbf{S} = \frac{1}{N}\sum_{s}^{N}\left(c_s[\mathbf{k}_i] - \bar{c}[\mathbf{k}_i]\right)\left(c_s[\mathbf{k}_i] - \bar{c}[\mathbf{k}_i]\right)^T. \quad (8)$$

Since most of the variation can be explained by a small number of eigenvectors, only a portion of the original set is kept, corresponding to the number of eigenvectors $t$ whose sum represents $90\%$ of the total variance of all variables. In this way, any shape from the dataset can be approximated by:

$$c[\mathbf{k}] \approx \bar{c}[\mathbf{k}] + \mathbf{P}\mathbf{b}, \quad (9)$$

where $\mathbf{P}$ is the matrix of the first $t$ eigenvectors and $\mathbf{b}$ is a vector of $t$ weights which for any given shape corresponds to $\mathbf{b} = \mathbf{P}^T\left(c[\mathbf{k}] - \bar{c}[\mathbf{k}]\right)$.

To be able to model both ED and ES separately, two different SSMs were created according to the methodology described above. The mean shapes for each of these models are shown in Figure 1. Note that since these models are scaled according to (6) only shape variations can be observed in this figure. Additional description of each of the SSMs, namely the shape variations described by each component, are provided in the supplementary files.

### C. SSM-Based Regularization

To then use the SSM with BEAS for the segmentation of new images, two different regularization energies were defined so that the segmented shapes are regularized according to those observed in the training set. These two regularizations, a hard and a soft SSM-based regularization, were first proposed by Queirós et al. [17]. In the present study, those regularization energies were adapted to regularize the B-spline coefficients $c[\mathbf{k}]$ of a 3D shape.

The hard SSM-based regularization restricts the segmented shape to the shape variability observed in the training set. At each iteration, the weights $\mathbf{b}$ are computed and each is restricted to $\pm m\sqrt{\lambda_i}$, where $m$ defines the limits to the variability from the mean [22]. $m$ is typically set between 2 and 3 since most of the population lies within three standard deviations and was set at 2.5 in this study. Through (9), a new regularized shape $c_{reg}[\mathbf{k}]$ is then obtained [17]. To include this hard SSM-based term in the BEAS framework, the energy functional can be defined as:

$$E_{hard} = \int_{\Gamma}\frac{1}{2}\left(c[\mathbf{k}] - c_{reg}[\mathbf{k}]\right)^2 d\mathbf{x}^*. \quad (10)$$

The minimization of this energy according to the B-spline coefficients gives:

$$\frac{\partial E_{hard}}{\partial c[\mathbf{k}]} = \int_{\Gamma}\left(c[\mathbf{k}] - c_{reg}[\mathbf{k}]\right) d\mathbf{x}^*. \quad (11)$$

The soft SSM-based regularization follows the rationale that it is much more probable to find an average shape than a shape which is close to the variability limits. In that way, the soft SSM-based regularization penalizes high values of $b_i$ and is defined as the squared Mahalanobis distance to the training shapes [22], thus:

$$E_{soft} = \sum_{i=1}^{t}\frac{b_i^2}{\lambda_i} = \int_{\Gamma}\left(c[\mathbf{k}] - \bar{c}[\mathbf{k}]\right)^T\mathbf{S}^{-1}\left(c[\mathbf{k}] - \bar{c}[\mathbf{k}]\right) d\mathbf{x}^* \quad (12)$$

Following the derivation shown in Queirós et al. [17], the minimization of $E_{soft}$ gives:

$$\frac{\partial E_{soft}}{\partial c[\mathbf{k}]} = \int_{\Gamma} 2\mathbf{P}\mathbf{D}^{-1}\mathbf{b}\, d\mathbf{x}^*, \quad (13)$$

where $\mathbf{D}$ is the diagonal matrix of $t$ eigenvalues $\lambda$.

To incorporate these two energies into BEAS, the regularization term $E_r$ is defined as:

$$E_r = \alpha E_{hard} + \beta E_{soft}, \quad (14)$$

where $\alpha$ and $\beta$ are hyperparameters controlling the relative weight between the two terms.

### D. Framework Description

A conceptual description of the proposed framework is shown in Figure 2.

*1) Automatic Initialization:* The automatic initialization algorithm used was first introduced in Barbosa et al. [19] and was inspired by the work of van Stralen et al. [24]. It relies on the sequential detection of the LV long axis (LAx) and the base to fit a spheroid to the endocardial boundaries. A detailed description of this method can be found in the original paper by Barbosa et al. [19]. This initialization will provide the initial estimation of the LAx and center for BEAS and the SSM.

*2) Automatic SAx Orientation:* The short axis (SAx) orientation method used was proposed in Pedrosa et al. [25]. This method aims at the detection of the right ventricular inferior insertion point and relies on image intensity information and analysis of the structures surrounding the LV. A detailed description of this method can be found in Pedrosa et al. [25].

The SAx orientation is crucial to correctly position the SSM, given that different sides of the LV have different shape characteristics. However, this orientation algorithm depends on a previous estimate of the LV surface and the result from the initialization is too rough as it relies on the fitting of an ellipsoid. As such, the automatic SAx orientation is only applied after an initial stage of segmentation with BEAS.

*3) Segmentation at ED:* The segmentation at ED is composed of two stages. Initially, BEAS is used without the SSM, so that the energy criterion $E$ is equal to $E_d$, the data attachment term. This provides an initial segmentation of the LV, which is used for the SAx orientation estimation but also to refine the initial estimates of LAx orientation and center

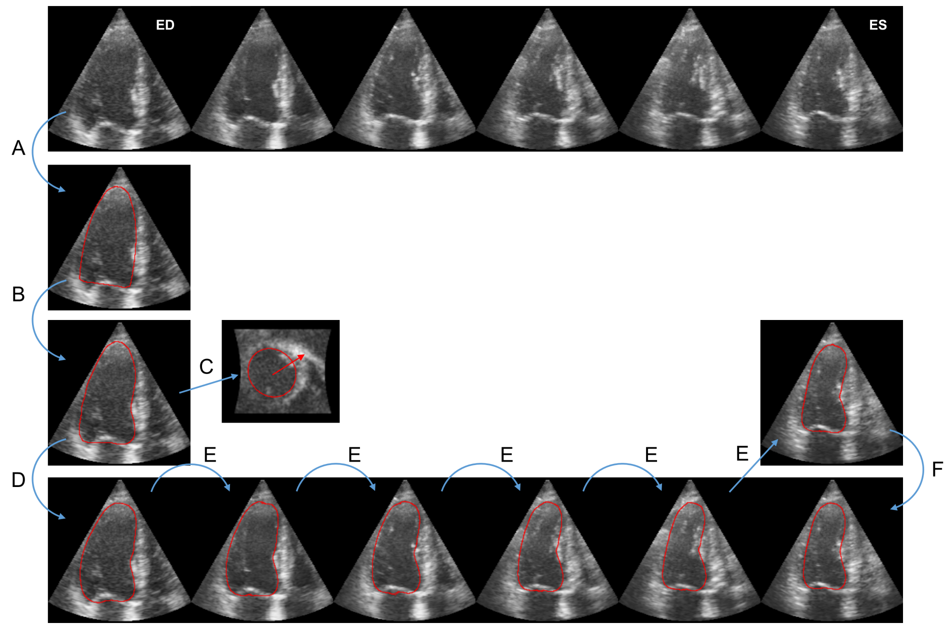


Fig. 2: Conceptual description of the proposed segmentation and tracking framework. First, automatic initialization is applied to the ED frame (A). The first stage of segmentation is then performed using BEAS (B). The result from this segmentation is used to detect the SAx orientation (C) and this information is then used to perform the second stage of segmentation using BEAS and the ED SSM. The final ED segmentation is then propagated frame to frame using the lAAOF (E) and a final refinement to the ES frame is performed using BEAS and the ES SSM (F).

according to the centroid and direction of largest variance of the segmented mesh. With the center position and both the LAx and SAx orientation well defined, it is then possible to use BEAS with the SSM regularization according to (14) to further refine the segmentation.

*4) Localized Anatomical Affine Optical Flow (lAAOF):* lAAOF is then used to propagate the result from ED to the remaining frames. The lAAOF method was proposed in Queirós et al. [18] and relies on an affine optical flow approach which independently estimates the motion at each point in the surface based on an anatomically constrained neighborhood. A detailed description of this method can be found in the original paper by Queirós et al. [18]. The parameters used to tune the lAAOF were replicated from [18].

*5) Segmentation at ES:* Segmentation at ES is used to further refine the result from the lAAOF, thus bringing together intensity and shape-based clues. In order to balance the contribution between tracking and segmentation clues, an energy term was added to penalize the deviation between the result of the lAAOF and the segmentation. Such an approach was first proposed by Barbosa et al. in [26] and can be formulated as:

$$E_A = \int_\Gamma \left(\psi(\mathbf{x}^*) - \tilde{\psi}(\mathbf{x}^*)\right)^2 \, d\mathbf{x}^*, \tag{15}$$

where $\tilde{\psi}(\mathbf{x}^*)$ is the surface obtained from the tracking using lAAOF. The minimization of this energy with regard to the B-spline coefficients can be performed according to:

$$\frac{\partial E_A}{\partial c[\mathbf{k}]} = \int_\Gamma 2\left(\psi(\mathbf{x}^*) - \tilde{\psi}(\mathbf{x}^*)\right)\beta^d\left(\frac{\mathbf{x}^*}{h} - \mathbf{k}_i\right) d\mathbf{x}^*. \tag{16}$$

The regularization energy criterion is then expressed as:

$$E_r = \alpha E_{hard} + \beta E_{soft} + \gamma E_A, \tag{17}$$

where $\gamma$ is a hyperparameter used to define the balance between tracking and intensity/shape-based information.

## III. Experiments

### A. Data Description

The proposed framework was tested on the CETUS challenge data [8]. This challenge comprises 45 sequences of 3D ultrasound volumes of one cardiac cycle from 45 patients acquired in three different hospitals and ultrasound machines from three different vendors. On each dataset, the LV endocardium was contoured by three experts at ED and ES until consensus was achieved between the three. Fifteen datasets are available as training with the corresponding reference meshes at ED and ES, while the remaining 30 datasets correspond to the testing set and only the 3D echocardiographic images are available.

### B. Segmentation Performance

First, the 15 training datasets were used to tune the hyperparameters $\beta$ and $\gamma$ needed respectively for the SSM regularization and for the balance between the segmentation and tracking information. This tuning was performed empirically by visual inspection of the results. The hyperparameters $\alpha$, $\beta$ and $\gamma$ were set respectively to 1, 0.0005 and 0.25. Note that the value of $\beta$ is directly related to the absolute value of eigenvalues $\lambda$ as defined in (12), thus justifying its relative small value.

Using these settings, the framework was then tested on the 30 testing datasets. The evaluation of the results was conducted using the online MIDAS platform of the CETUS challenge, thus assuring that the proposed method can be directly compared to other state-of-the-art methods. The accuracy of the segmentation was evaluated at ED and ES through different distance metrics: Mean Absolute Distance (MAD) [27], which measures the average distance at any point between the segmented and reference meshes; Hausdorff Distance (HD) [28], which measures the maximum distance between the segmented and reference meshes; and Dice [29], which is a measure of the overlap between the segmented and reference meshes. Because the meshes obtained from BEAS are sampled in the spherical coordinate system, causing the point density to be different along the surface, which could bias the error metrics to specific regions, the segmented meshes were remeshed to assure greater smoothness and more uniform mesh point density. Clinical indices were also studied, namely the Pearson correlation coefficient and limits of agreement of ED volume (EDV), ES volume (ESV) and ejection fraction (EF).

Mean computational times of the proposed framework were also obtained using MATLAB code running on an Intel® Xeon® E5-1650v2@3.5GHz with 32GB RAM.

### C. Position/Orientation Performance and Sensitivity

Because the characteristics of the SSM are closely related to the position and orientation (LAx and SAx) of the BEAS coordinate system, it is important to determine the error in the estimation of these parameters. For that purpose, the position, LAx orientation and SAx orientation of the CETUS training set reference meshes were compared to those obtained with the proposed method.

Furthermore, the sensitivity of the segmentation results to variations of these parameters was studied. This was performed by introducing variations from the reference position or orientation on each of these parameters and evaluating the segmentation performance. In this way, to evaluate, for example, the sensitivity to the position, BEAS was initialized at a random position at a distance $D$ from the reference mesh position and with the reference SAx and LAx orientation. The segmentation result was then evaluated on MAD, HD and Dice. To prevent sporadic results from this random positioning, each image was started from three different random positions each time and the results averaged.

### D. Parameter Sensitivity Assessment

To study the robustness and stability of the proposed framework with respect to the multiple parameters involved, a parameter sensitivity assessment was conducted. As such, the balance of the different energies, namely $\alpha$, $\beta$ and $\gamma$, was studied. Each parameter was varied from their empirically determined preset by $50\%$ of its value and its impact studied in terms of MAD, HD and Dice. To further analyse the contribution of each component of the framework, the segmentation performance was analysed when each of these energy parameters was set to zero. To highlight the importance of the lAAOF, the segmentation performance of the framework without the lAAOF was also studied by using the ED segmentation result for initialization of the ES segmentation.

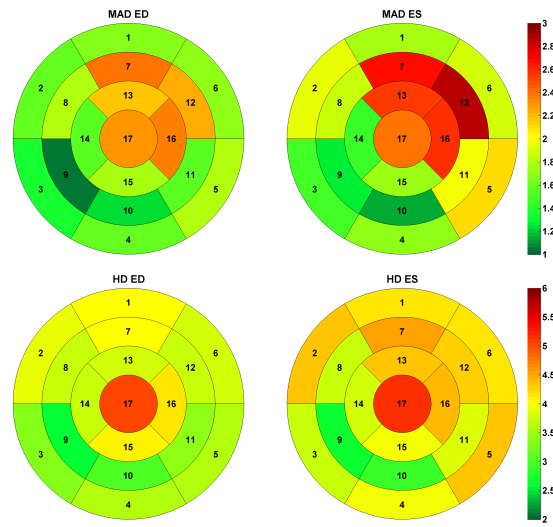


Fig. 3: Bullseye plots of average MAD and HD at every region for ED and ES for the training datasets. Measures in mm.

### E. Statistical Analysis

Paired t-tests were used to analyse the significance of differences between the proposed method and other methods in literature and to analyse the parameter sensitivity of the proposed method. Results are denoted as mean ± standard deviation.

## IV. Results

.

### A. Segmentation Performance

Tables I and II show the segmentation and tracking results for the proposed approach, as well as the performance obtained with other state-of-the-art methods and inter-observer variability from manual contouring. Those obtained by Queirós et al. [18] and Barbosa et al. [9] also use BEAS as the segmentation tool but neither use shape-based information. Queirós et al. used the same lAAOF tracking whereas Barbosa et al. used a global anatomically constrained optical flow approach followed by block matching refinement instead of the lAAOF. The other approaches presented were chosen as they are, to the author's knowledge, the ones presenting the best segmentation results on the CETUS dataset.

A regionwise analysis of error was also conducted by dividing the LV into the 17-segment model [31], using the LAx as reference and dividing the LV into basal (35%), mid-cavity (35%) and apical (30%) regions. The average MAD and HD at ED and ES for the training datasets is shown in Figure 3. It can be observed that the greatest errors occur on the apical region and on the anterior side of the LV. Figure 4 shows examples of the fully automatic segmentation results compared to the consensus manual contours by experts.

TABLE I: Performance on the CETUS testing datasets. MAD, HD and Dice of the proposed framework, other state-of-the-art approaches and inter-observer variability. All values in mean $\pm$ standard deviation ($NR$ stands for not reported). $\star$, † and ‡ indicate respectively that the difference to the proposed framework was statistically significant at a $p<0.05$, $p<0.01$ and $p<0.001$ level. Note that for methods [10], [15], [14], [30] a comparison is not possible as the data is not publicly available.

| Method | MAD (mm) | | HD (mm) | | Dice | |
|---|---|---|---|---|---|---|
| | ED | ES | ED | ES | ED | ES |
| Proposed | $1.81 \pm 0.59$ | $1.98 \pm 0.66$ | $6.31 \pm 1.69$ | $6.95 \pm 2.14$ | $0.909 \pm 0.034$ | $0.875 \pm 0.046$ |
| Queirós et al. [18] | $2.26 \pm 0.72^{\ddagger}$ | $2.45 \pm 0.85^{\ddagger}$ | $8.10 \pm 2.62^{\ddagger}$ | $8.19 \pm 3.03^{\star}$ | $0.894 \pm 0.040^{\ddagger}$ | $0.861 \pm 0.054^{\star}$ |
| Barbosa et al. [9] | $2.26 \pm 0.72^{\ddagger}$ | $2.43 \pm 0.89^{\ddagger}$ | $8.10 \pm 2.62^{\ddagger}$ | $8.29 \pm 3.01^{\star}$ | $0.894 \pm 0.040^{\ddagger}$ | $0.856 \pm 0.056^{\ddagger}$ |
| Bernier et al. [10] | $2.37 \pm NR$ | $2.64 \pm NR$ | $9.41 \pm NR$ | $9.34 \pm NR$ | $0.882 \pm NR$ | $0.837 \pm NR$ |
| van Stralen et al. [15] | $1.91 \pm NR$ | $2.48 \pm NR$ | $6.66 \pm NR$ | $7.38 \pm NR$ | $0.910 \pm NR$ | $0.862 \pm NR$ |
| Oktay et al. [14] | $1.94 \pm 0.55$ | $2.23 \pm 0.60$ | $7.00 \pm 1.99$ | $7.53 \pm 2.23$ | $0.904 \pm 0.02$ | $0.874 \pm 0.04$ |
| Inter-observer Variability [30] | $1.01 \pm 0.30$ | $1.01 \pm 0.38$ | $3.37 \pm 0.87$ | $3.30 \pm 0.94$ | $0.949 \pm 0.15$ | $0.938 \pm 0.21$ |

TABLE II: Performance on the CETUS testing datasets. Pearson correlation coefficient (R) and limits of agreement (LOA) (mean $\pm$ standard deviation) in comparison to the reference cardiac indices (EDV, ESV and EF) of the proposed framework, other state-of-the-art approaches and inter-observer variability. Volumes obtained with the proposed method were not statistically significantly different at a $p<0.05$ level when compared to [18], [9]. Note that for methods [10], [15], [14], [30] a comparison is not possible as the data is not publicly available.

| Method | EDV (ml) | | ESV (ml) | | EF (%) | |
|---|---|---|---|---|---|---|
| | R | LOA | R | LOA | R | LOA |
| Proposed | 0.953 | $-3.29 \pm 19.03$ | 0.960 | $-4.84 \pm 16.09$ | 0.911 | $1.7 \pm 5.18$ |
| Queirós et al. [18] | 0.965 | $-4.99 \pm 17.66$ | 0.971 | $-5.83 \pm 13.14$ | 0.927 | $2.30 \pm 4.20$ |
| Barbosa et al. [9] | 0.965 | $-4.99 \pm 17.66$ | 0.967 | $-6.78 \pm 13.86$ | 0.889 | $2.88 \pm 5.24$ |
| Bernier et al. [10] | 0.979 | $2.74 \pm 13.87$ | 0.968 | $2.18 \pm 13.73$ | 0.811 | $0.05 \pm 7.84$ |
| van Stralen et al. [15] | 0.958 | $-4.86 \pm 18.08$ | 0.965 | $-15.39 \pm 15.08$ | 0.751 | $8.40 \pm 7.72$ |
| Oktay et al. [14] | 0.961 | $-4.14 \pm 17.35$ | 0.973 | $-3.47 \pm 13.62$ | 0.892 | $0.48 \pm 5.50$ |
| Inter-observer Variability [30] | 0.981 | $-0.64 \pm 9.27$ | 0.987 | $-0.50 \pm 7.35$ | 0.959 | $0.13 \pm 3.10$ |

Regarding computational time, the proposed framework took on average 0.9 s for the initialization, 0.6 s for the SAx orientation and a combined time of 1.1 s for the two stages of ED segmentation. The tracking took on average 0.8 s/frame and the final ES segmentation 0.4 s. The total time for a fully automatic ED/ES segmentation was on average 11 s. All data was processed in a non-optimized MATLAB implementation.

### B. Position/Orientation Performance and Sensitivity

At initialization, the position and LAx orientation errors were respectively $3.7{\pm}2.1$ mm and $5.0{\pm}2.8°$. After refinement at the first stage of ED BEAS segmentation, the position and LAx orientation errors were reduced to respectively $2.4 \pm 1.0$ mm and $4.4{\pm}2.4°$. Automatic SAx orientation failed in one of the cases due to low image quality giving an error of $120.2°$ compared to manual annotation of the RV insertion point. On the remaining datasets the SAx orientation error was $6.9{\pm}4.4°$.

Figure 5 shows the influence on the segmentation performance of the position and orientation of the automatically defined BEAS coordinate system with respect to the position and orientation of the reference meshes. It can be observed that the position and LAx orientation have the most influence on the segmentation results, where a distance above 2mm from the reference mesh centroid or an LAx angle deviation greater than $8°$ give an error larger than what was obtained with the fully automatic method used in this study.

### C. Parameter Sensitivity Assessment

Figure 6 shows the influence of the parameters $\alpha$, $\beta$ and $\gamma$ on the segmentation results at ED and ES. For the interval considered from $50\%$ to $150\%$ of the preset value, none of the observed changes were statistically significant at a $p<0.01$ level and only the MAD at ES showed several statistically significant changes at a $p<0.05$ level when changing $\beta$. When parameters $\beta$ and $\gamma$ are set to 0, the difference is statistically significant at a $p<0.001$ level whereas for $\alpha$ the difference is not statistically significant. When removing the lAAOF, the ES segmentation presents an MAD, HD and Dice of $2.91 \pm 1.08$mm, $9.81 \pm 2.92$mm and $0.861 \pm 0.054$ respectively (all statistically significant at a $p<0.001$ level).

## V. Discussion

A fully automatic LV segmentation and tracking framework is proposed, combining the strengths of image information from BEAS and shape-based clues from an SSM for segmentation and lAAOF to perform tracking. The way in which the SSM is represented on the BEAS space, through the corresponding B-spline representation coefficients $c[\mathbf{k}]$, brings BEAS and the SSM closer together, avoiding steps such as conversion between the spherical and Cartesian coordinate systems and scaling/translation operations. It also avoids one of the fundamental problems with SSM, the point correspondence between different training shapes and with testing shapes. This approach assumes however that the position and orientation

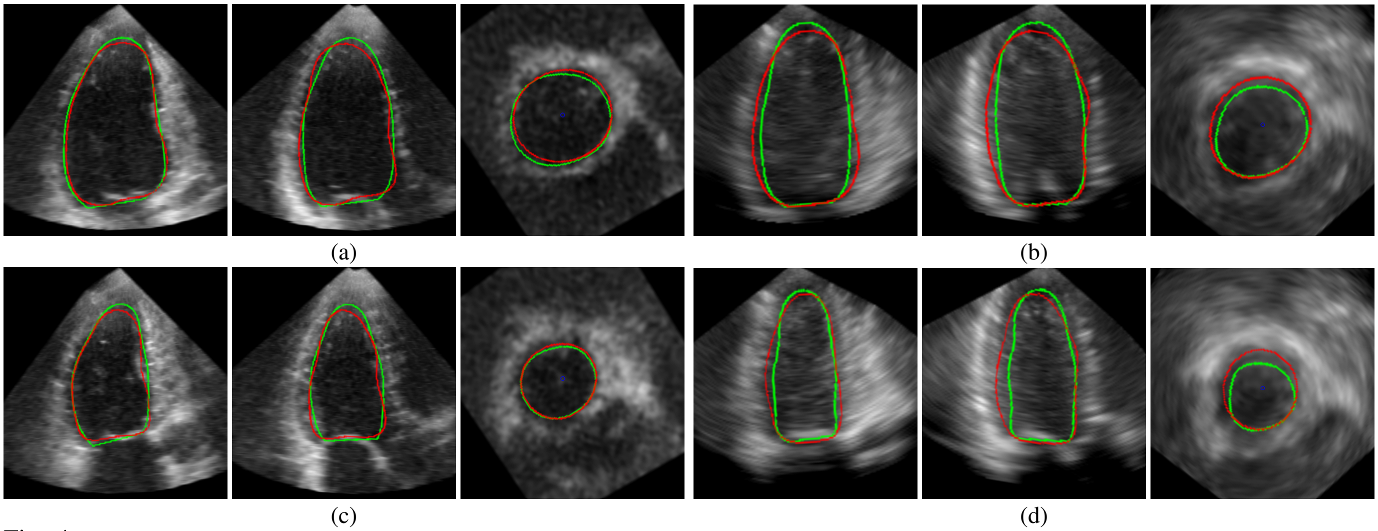


Fig. 4: Best (a,c) and worst (b,d) automatic segmentation results (red) compared to manual contours by experts (green) at ED (top row) and ES (bottom row) from the CETUS training set. The three orthogonal planes shown for each 3D image were chosen according to the automatically defined LAx/SAx orientation.

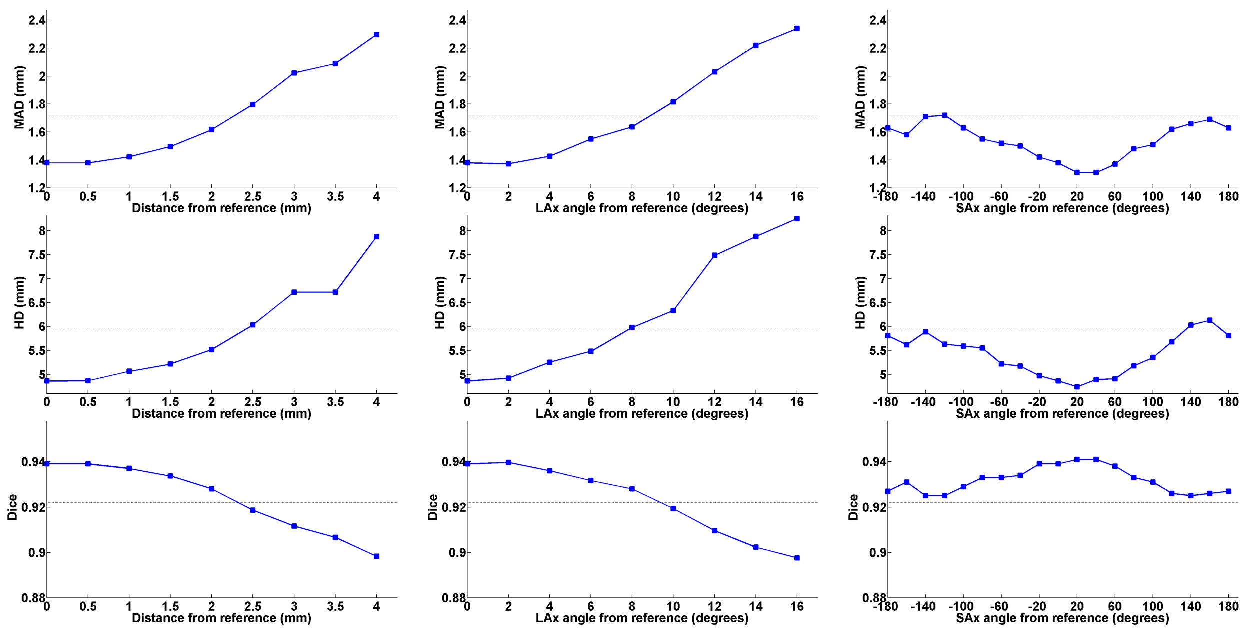


Fig. 5: Influence of the distance and angle error from the reference position and orientation on the distance metrics (MAD, HD and Dice) at ED. Horizontal dotted line indicates the performance obtained with the proposed automatic framework on the CETUS training set.

of the coordinate system is identical for every shape. For the training shapes, it is trivial to match the position and orientation of every shape, making the previous assumption valid. When trying to fit the SSM to a new image, the center and both the LAx and SAx orientations have to be guessed from image features.

### A. *Segmentation Performance*

From Table I it is clear that the proposed automatic method shows excellent segmentation and tracking performance and outperforms any other of the state-of-the-art approaches applied to the same database. Compared to other approaches using BEAS [18], [9], the impact of the SSM regularization on ED segmentation is statistically significant. With a better starting point at ED for the lAAOF, together with the SSM regularization at ES, the ES segmentation results are also improved, thereby outperforming other state-of-the-art methods. Given the different strategies used in each framework, it is difficult to say with certainty what is the reason behind the differences in performance but the following possible reasons can be considered: regarding the semi-automatic method of Bernier et al. [10] using graph cuts, this method lacks a source of prior information needed to give an accurate segmentation when image information is low or incongruous. For both van Stralen et al. [24] and Oktay et al. [14] that information is provided, respectively, by an active appearance model and a multi-atlas approach. However, both these approaches use ultrasound data as a prior which can be more variable than

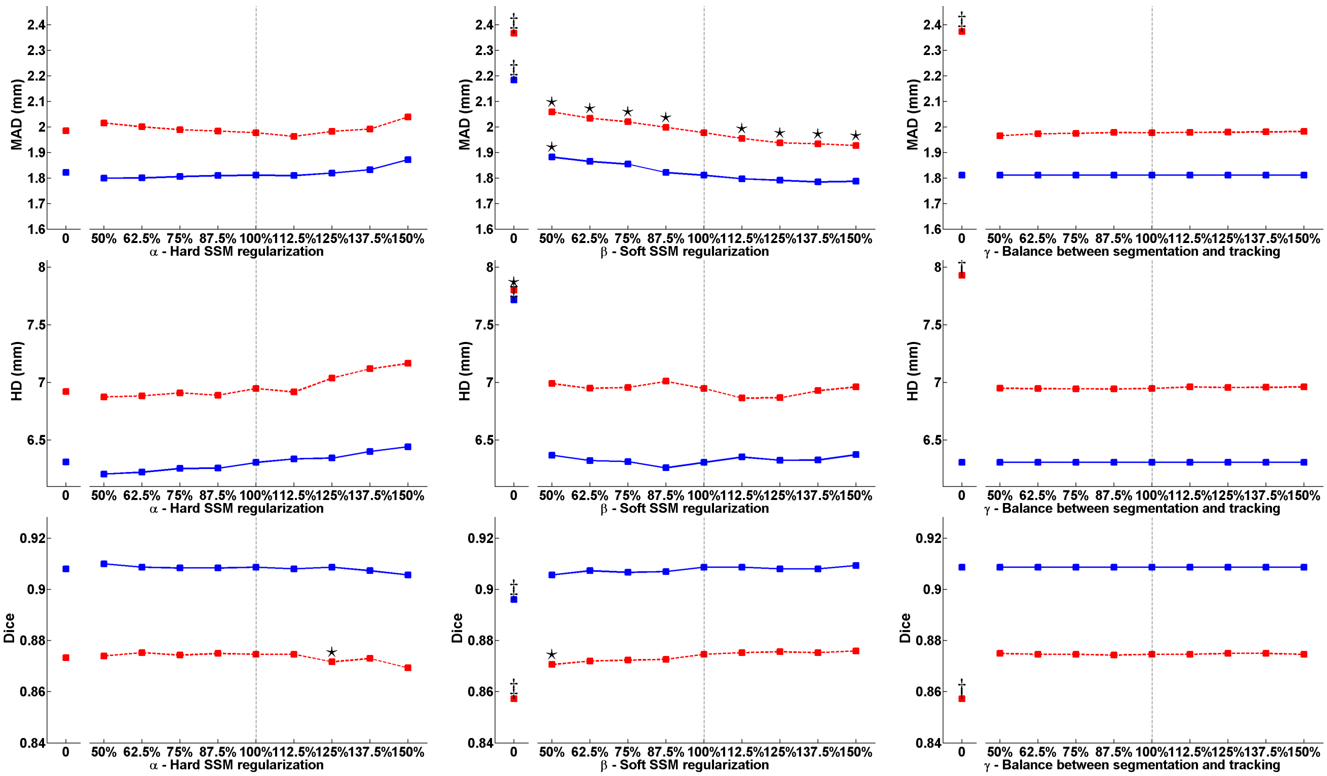

Fig. 6: Influence of the variation of each of the considered parameters $\alpha$, $\beta$ and $\gamma$ on the distance metrics (MAD, HD and Dice) at ED (blue) and ES (red dotted). Vertical dotted line indicates the preset parameter value. $\star$, † and ‡ indicate respectively that the difference to the result with the preset values was statistically significant at a $p<0.05$, $p<0.01$ and $p<0.001$ level.

cMR, especially for reduced datasets. Moreover, both these methods intend to model the appearance of the image, which can be particularly difficult due to the differences between vendors, bad acquisition window or the presence of artifacts. Regarding the clinical indices on Table II, the proposed method has a performance similar to the remaining state-of-the-art methods.

Regarding the regionwise analysis shown in Figure 3, there could be two possible explanations for the regions with larger error: either there are inherent image characteristics that make segmentation more difficult or there are framework specific characteristics that cause these errors, such as a systematic error on the LAx detection. However, regionwise error analysis in different frameworks and on manual contouring by experts replicate this trend of larger errors at the apical and anterolateral regions [8], which points to inherent image characteristics that make the segmentation more difficult. Indeed, at the apex, image information is low due to noise in the near field, whereas for the anterolateral region, dropout in this region is common due to its position and proximity to lung tissue.

As for the computational speed, the proposed framework continues to be computationally efficient, especially if compared to other state-of-the-art approaches. Oktay et al. [14] reported an average time of 16min per image and Van Stralen et al. [24] reported an average segmentation time of 15s in a C++ environment [32] to which the tracking time must be added (not reported). Furthermore, one can consider ways of decreasing the computational burden of the proposed method by changing to a more efficient implementation in C++, where it has been shown that 3D endocardial segmentation can be done using BEAS in approximately 12.5 ms [16].

### B. *Position/Orientation Performance and Sensitivity*

As predicted, moving the position and orientation away from the reference has a strong impact on the performance. The fact that SAx orientation has a smaller effect than center position and LAx orientation can be explained by the fact that, though the LV is far from being symmetric, the shape differences between the different sides are much less pronounced than the shape difference between the apex and base of the LV or those resulting from representing the LV shape from a wrong position. As such, a compromise between the image information and the SSM can more easily be found for an incorrect SAx orientation than from an incorrect center position or LAx orientation.

Figure 5 also shows that one of the bottlenecks of this method is the positioning and orientation of the LV. It can be seen that when the reference position and orientation is used, the error decreases considerably (MAD: 1.38 mm; HD: 4.86 mm; Dice: 0.959). As such, it would be important, in future work, to focus on better automatic initialization methods that, ideally, would provide the true center of the LV and the LAx and SAx orientation. This would imply however to move away from the current initialization, which roughly delineates the LV using the Hough transform, to more complex methodologies, possibly involving machine learning or other more abstract approaches.

### C. Parameter Sensitivity Assessment

Overall, the parameter sensitivity assessment showed that the performance of the proposed method is not significantly impaired within a wide range of the parameter settings. The parameters related to the SSM regularization seem to have a higher impact as they control the balance between the image information and the SSM. The parameter related to the balance between segmentation and tracking has, as expected, no impact on ED segmentation since $\gamma$ is not used at ED, and little impact on ES segmentation performance. When each of the parameters is set to zero, thus turning off the corresponding energy contribution, the performance contribution of each energy becomes clear and both $\beta$ and $\gamma$ are crucial for the results obtained. The contribution of $\alpha$ is, however, less pronounced. This is due to the fact that the soft energy term already penalizes shapes away from the mean shape, making it less likely for the segmented shape to deviate to the hard set limits at $m = 2.5$. Nevertheless, it can be argued that the hard energy term is important to effectively limit the maximum deviation from the mean shape (if $\alpha = 1$) and in more challenging images where image artifacts could make it easier for the segmented shape to deviate from the mean.

Regarding the lAAOF, it is shown that it also plays an important role in following the endocardial surface from ED to ES to initialize the segmentation at ES, as the results without the lAAOF are significantly worse than the proposed method. Nevertheless, in spite of the fact that in this study the lAAOF was chosen to track the endocardial surface, other tracking methods could equally be applied in a straightforward manner and, if proven to be more effective in tracking the LV, could potentially improve the ES segmentation results further.

Though in this study only the parameters related to the balance of the different energies were studied, the performance of BEAS and the lAAOF also depend on different parameters. Nonetheless, these have been studied before [19], [33], [18] and the optimal settings found were used in this study.

### D. Limitations and Future Work

In spite of the promising results shown in this paper, there are limitations which must be addressed in the future. First, as mentioned in Section V-B, the positioning and orientation of the LV is a limiting factor of the accuracy of the proposed framework and should be addressed in the future to provide better segmentation results. Secondly, the parameter tuning performed in this study was quite limited. While in this study only parameters $\beta$ and $\gamma$ were subject to parameter tuning, there are other parameters that could be further tuned and which were not directly addressed. Even though some of these have been tuned before on the same dataset such as the BEAS [9] and lAAOF [18] parameters, a tuning of all parameters together could prove beneficial, especially for the framework elements identified as crucial such as the initialization. Thirdly, in this study only the endocardial border was considered. Nevertheless, the epicardial border is also of importance to study clinical indices, such as LV mass, and is an essential step for automatic cardiac strain measurements through the definition of a region-of-interest. As such, it would be interesting to build an SSM that would describe both the endo- and epicardial borders so that the current framework could be applied for full myocardial segmentation. However, the validation of such a framework cannot be done with the CETUS challenge dataset, as no epicardial contours are provided and, to the author's knowledge, there are no other freely available and reliable datasets of 3D ultrasound data with both endo- and epicardial manual contours.

The dataset used for the SSM must also be considered. First, it could be argued that the cMR shapes used are not ideal as they are derived from 2D slices rather than from true 3D data. However, that would imply that replacing the current SSM by one built from true 3D data would only further improve the results as more accurate data would be embedded into the SSM. Secondly, the very population targeted by the study from where the shapes were obtained is not ideal. Given that DOPPLER-CIP targeted patients suspected of chronic ischemic disease, one cannot consider that the dataset used represents a normal population. However, as before, that would imply that replacing this population with a more representative one would only improve results as the SSM is more well suited for the purpose for which it is intended.

## VI. Conclusion

In this work, a novel fast and fully automatic LV segmentation and tracking framework based on shape-based BEAS and lAAOF is proposed. The proposed approach outperforms all other state-of-the-art methods for LV segmentation evaluated on the MICCAI CETUS challenge. Moreover, it outperforms other methods in terms of computational speed, being able to perform ED/ES segmentation and tracking in a few seconds in a non-optimized implementation. The main strengths of the proposed framework result from the combination of image and shape information through the balance of the image information from BEAS and the SSM regularization and the combination of tracking and segmentation clues for an efficient ES segmentation.

## Acknowledgments

This work was made possible through funding from the European Research Council under the European Unions Seventh Framework Program (HeartMAPAS; FP7/2007-2013/ERC Grant Agreement number 281748) and from FCT Fundação para a Ciência e a Tecnologia, Portugal, in the scope of the PhD Grant SFRH/BD/93443/2013.

## References

[1] P. M. Elliott, A. Anastasakis, M. A. Borger, M. Borggrefe, F. Cecchi, P. Charron, A. A. Hagege, A. Lafont, G. Limongelli, H. Mahrholdt *et al.*, "2014 ESC guidelines on diagnosis and management of hypertrophic cardiomyopathy: The task force for the diagnosis and management of hypertrophic cardiomyopathy of the european society of cardiology (ESC)," *European Heart Journal*, vol. 35, no. 39, p. 2733, 2014.

[2] R. A. Nishimura, C. M. Otto, R. O. Bonow, B. A. Carabello, J. P. Erwin, R. A. Guyton, P. T. O'Gara, C. E. Ruiz, N. J. Skubas, P. Sorajja *et al.*, "2014 AHA/ACC guideline for the management of patients with valvular heart disease," *Journal of the American College of Cardiology*, vol. 63, no. 22, pp. e57–e185, 2014.

[3] C. W. Yancy, M. Jessup, B. Bozkurt, J. Butler, D. E. Casey, M. H. Drazner, G. C. Fonarow, S. A. Geraci, T. Horwich, J. L. Januzzi *et al.*, "2013 ACCF/AHA guideline for the management of heart failure," *Circulation*, vol. 128, no. 16, pp. e240–e327, 2013.

[4] K. E. Leung and J. G. Bosch, "Automated border detection in three-dimensional echocardiography: principles and promises," *European Journal of Echocardiography*, vol. 11, no. 2, p. 97, 2010.

[5] J. Pedrosa, D. Barbosa, N. Almeida, O. Bernard, J. Bosch, and J. D'hooge, "Cardiac chamber volumetric assessment using 3D ultrasound - a review," *Current Pharmaceutical Design*, vol. 22, no. 1, pp. 105–121, 2016.

[6] N. Almeida, D. Friboulet, S. I. Sarvari, O. Bernard, D. Barbosa, E. Samset, and J. Dhooge, "Left-atrial segmentation from 3-d ultrasound using b-spline explicit active surfaces with scale uncoupling," *IEEE Transactions on Ultrasonics, Ferroelectrics, and Frequency Control*, vol. 63, no. 2, pp. 212–221, Feb 2016.

[7] X. Qin, Z. Cong, and B. Fei, "Automatic segmentation of right ventricular ultrasound images using sparse matrix transform and a level set," *Physics in medicine and biology*, vol. 58, no. 21, p. 7609, 2013.

[8] O. Bernard, J. G. Bosch, B. Heyde, M. Alessandrini, D. Barbosa, S. Camarasu-Pop, F. Cervenansky, S. Valette, O. Mirea, M. Bernier *et al.*, "Standardized evaluation system for left ventricular segmentation algorithms in 3D echocardiography," *IEEE Transactions on Medical Imaging*, vol. 35, no. 4, pp. 967–977, April 2016.

[9] D. Barbosa, D. Friboulet, J. D'hooge, and O. Bernard, "Fast tracking of the left ventricle using global anatomical affine optical flow and local recursive block matching," *The MIDAS Journal*, 10 2014.

[10] M. Bernier, P. Jodoin, and A. Lalande, "Automatized evaluation of the left ventricular ejection fraction from echocardiographic images using graph cut," *The MIDAS Journal*, 10 2014.

[11] O. Oktay, W. Shi, K. Keraudren, J. Caballero, and D. Rueckert, "Learning shape representations for multi-atlas endocardium segmentation in 3D echo images," *The MIDAS Journal*, 10 2014.

[12] C. Wang and O. Smedby, "Model-based left ventricle segmentation in 3D ultrasound using phase image," *The MIDAS Journal*, 10 2014.

[13] E. Smistad and F. Lindseth, "Real-time tracking of the left ventricle in 3D ultrasound using kalman filter and mean value coordinates," *The MIDAS Journal*, 10 2014.

[14] O. Oktay, A. Gomez, K. Keraudren, A. Schuh, W. Bai, W. Shi, G. Penney, and D. Rueckert, *Probabilistic Edge Map (PEM) for 3D Ultrasound Image Registration and Multi-atlas Left Ventricle Segmentation*. Cham: Springer International Publishing, 2015, pp. 223–230.

[15] M. van Stralen, A. Haak, K. Y. E. Leung, G. van Burken, C. Bos, and J. G. Bosch, "Full-cycle left ventricular segmentation and tracking in 3D echocardiography using active appearance models," in *2015 IEEE International Ultrasonics Symposium (IUS)*, Oct 2015, pp. 1–4.

[16] D. Barbosa, T. Dietenbeck, J. Schaerer, J. D'hooge, D. Friboulet, and O. Bernard, "B-spline explicit active surfaces: An efficient framework for real-time 3-D region-based segmentation," *IEEE Transactions on Image Processing*, vol. 21, no. 1, pp. 241–251, Jan 2012.

[17] S. Queirós, A. Papachristidis, D. Barbosa, K. C. Theodoropoulos, J. C. Fonseca, M. J. Monaghan, J. L. Vilaça, and J. D'hooge, "Aortic valve tract segmentation from 3D-TEE using shape-based B-spline explicit active surfaces," *IEEE Transactions on Medical Imaging*, vol. 35, no. 9, pp. 2015–2025, Sept 2016.

[18] S. Queirós, J. L. Vilaça, P. Morais, J. C. Fonseca, J. D'hooge, and D. Barbosa, "Fast left ventricle tracking using localized anatomical affine optical flow," *International Journal for Numerical Methods in Biomedical Engineering*, pp. n/a–n/a, 2017, cnm.2871.

[19] D. Barbosa, T. Dietenbeck, B. Heyde, H. Houle, D. Friboulet, J. D'hooge, and O. Bernard, "Fast and fully automatic 3-D echocardiographic segmentation using B-spline explicit active surfaces: Feasibility study and validation in a clinical setting," *Ultrasound in Medicine & Biology*, vol. 39, no. 1, pp. 89 – 101, 2013.

[20] F. Rademakers, J. Engvall, T. Edvardsen, M. Monaghan, R. Sicari, E. Nagel, J. Zamorano, H. Ukkonen, T. Ebbers, V. Di Bello *et al.*, "Determining optimal noninvasive parameters for the prediction of left ventricular remodeling in chronic ischemic patients," *Scandinavian Cardiovascular Journal*, vol. 47, no. 6, pp. 329–334, Dec. 2013.

[21] P. J. Besl and N. D. McKay, "A method for registration of 3-D shapes," *IEEE Transactions on Pattern Analysis and Machine Intelligence*, vol. 14, no. 2, pp. 239–256, Feb 1992.

[22] T. Cootes, C. Taylor, D. Cooper, and J. Graham, "Active shape models-their training and application," *Computer Vision and Image Understanding*, vol. 61, no. 1, pp. 38 – 59, 1995.

[23] I. Jolliffe, *Principal Component Analysis*. John Wiley & Sons, Ltd, 2014.

[24] M. van Stralen, K. Leung, M. Voormolen, N. de Jong, A. van der Steen, J. Reiber, and J. Bosch, "Time continuous detection of the left ventricular long axis and the mitral valve plane in 3-D echocardiography," *Ultrasound in Medicine & Biology*, vol. 34, no. 2, pp. 196 – 207, 2008.

[25] J. Pedrosa, B. Heyde, L. Heeren, J. Engvall, J. Zamorano, A. Papachristidis, T. Edvardsen, P. Claus, and J. D'hooge, "Automatic short axis orientation of the left ventricle in 3D ultrasound recordings," in *Proceedings SPIE Medical Imaging 2016*, vol. 9790, 2016, pp. 97 900E–97 900E–7.

[26] D. Barbosa, O. Bernard, B. Heyde, T. Dietenbeck, D. Friboulet, and J. D'hooge, "Hybrid energy approach for real-time B-spline explicit active tracking of surfaces (heartBEATS)," in *2013 IEEE International Ultrasonics Symposium (IUS)*, July 2013, pp. 663–666.

[27] V. Chalana, D. Linker, D. Haynor, and Y. Kim, "A multiple active contour model for cardiac boundary detection on echocardiographic sequences," *IEEE Transactions on Medical Imaging*, vol. 15, no. 3, pp. 290–298, Jun 1996.

[28] D. Huttenlocher, G. Klanderman, and W. Rucklidge, "Comparing images using the Hausdorff distance," *IEEE Transactions on Pattern Analysis and Machine Intelligence*, vol. 15, no. 9, pp. 850–863, Sep 1993.

[29] L. R. Dice, "Measures of the amount of ecologic association between species," *Ecology*, vol. 26, no. 3, pp. pp. 297–302, 1945.

[30] A. Papachristidis, M. Geleijnse, E. Galli, B. Heyde, M. Alessandrini, D. Barbosa, M. Monaghan, O. Bernard, J. D'hooge, and J. Bosch, "Clinical expert delineation of 3D left ventricular echocardiograms for the CETUS segmentation challenge," *The MIDAS Journal*, 10 2014.

[31] M. D. Cerqueira, N. J. Weissman, V. Dilsizian, A. K. Jacobs, S. Kaul, W. K. Laskey, D. J. Pennell, J. A. Rumberger, T. Ryan, and M. S. Verani, "Standardized myocardial segmentation and nomenclature for tomographic imaging of the heart," *Circulation*, vol. 105, no. 4, pp. 539–542, 2002.

[32] M. V. Stralen, A. Haak, K. Leung, G. V. Burken, and J. Bosch, "Segmentation of multi-center 3D left ventricular echocardiograms by active appearance models," *The MIDAS Journal*, 10 2014.

[33] J. Pedrosa, D. Barbosa, B. Heyde, F. Schnell, A. Rosner, P. Claus, and J. D. hooge, "Left ventricular myocardial segmentation in 3D ultrasound recordings: Effect of different endo- and epicardial coupling strategies," *IEEE Transactions on Ultrasonics, Ferroelectrics, and Frequency Control*, vol. PP, no. 99, pp. 1–1, 2016.